FEM based determination of real and complex elastic, dielectric and piezoelectric moduli in piezoceramic materials

Tom Lahmer, Manfred Kaltenbacher, *Member, IEEE,* Barbara Kaltenbacher, Reinhard Lerch, *Member, IEEE* and Erich Leder

***Abstract*— We propose an enhanced iterative scheme for the precise reconstruction of piezoelectric material parameters from electric impedance and mechanical displacement measurements. It is based on finite element simulations of the full three-dimensional piezoelectric equations, combined with an inexact Newton-iterative or nonlinear Landweber iterative inversion scheme. We apply our scheme to two piezoelectric materials and test its performance. For the first material the manufacturer provides a full data set, whereas for the second one, no material data set is available. For both cases, our inverse scheme, using electric impedance measurements as input data, performs well.**

***Index Terms*— Piezoelectricity, material parameter determination, inverse problem, finite element method**

I. Introduction

For the optimal design of piezoelectric devices, efficient numerical simulation tools have been developed, that avoid expensive and time-consuming experiments by numerically solving the mathematical formulation of the underlying physical model, i.e., the system of partial differential equations with appropriate boundary conditions. Among all methods, the Finite Element (FE) method has become the standard numerical calculation scheme for the computer simulation of technical systems (see, e.g., [1], [2]) and in special for piezoelectric systems (cf., e.g. [3]). The accuracy of these methods, however, relies heavily on the material parameters steering the interaction of mechanical and electrical quantities. So far, these parameters have been estimated by experiments on test samples, whose special shape allows simplifications in the model. Hence, explicit formulas for parameter extraction from resonance frequencies exist (cf., e.g., for loss-less models [4],[5] and [6], [7], [8], [9], [10] considering losses.). However, the results of these estimation formulas do not provide sufficiently precise information on the material coefficients, giving rise to inaccurate results in computational simulations. Therefore, it was our aim to propose and implement a computational scheme that enables the determination of the whole material parameter set being appropriate for FE simulations.

The paper is organized as follows. In Sec. II, we discuss the necessity of material parameters appropriate for FE simulations and why a pure experimental based material parameter determination is not sufficient. The FE method for the piezoelectric partial differential equations are briefly described in Sec. III, followed by Sec. IV and V presenting our inversion scheme and the sensitivity analysis. The computational aspects are discussed in Sec. VI. In Sec. VII we provide a detailed discussion of the results, when applying our inverse scheme to both piezoelectric material.

Manuscript received July 20, 2005; revised November 18, 2005.

T. Lahmer, M. Kaltenbacher, B. Kaltenbacher, R. Lerch and E. Leder are with the Department of Sensor Technology, University of Erlangen-Nuremberg, Germany.

II. Necessity of Parameter Adaption for FEM

The main difference between mathematical models which are involved in the determination of material tensors using well-known resonance methods and real world simulations is the difference in the assumed space dimension. Thus, a discrepancy in the exactness of the material parameters is present for the following reasons. Published data sets are always a collection of parameters determined from a set of mono-modal samples operating at different frequency ranges. However, due to frequency dependency, the parameter sets are never precise enough for three dimensional numerical computations. In addition, most experimental based determinations of piezoelectric material parameters extract the data in the $(\mathbf{s}^{\mathbf{E}}, \mathbf{d}, \varepsilon^{\mathbf{T}})$ form. For a standard FE implementation, the $(\mathbf{c}^{E}, \mathbf{e}, \varepsilon^{S})$ form is required (see Sec. III). Each conversion of the data sets form the $(\mathbf{s}^{\mathbf{E}}, \mathbf{d}, \varepsilon^{\mathbf{T}})$ to the $(\mathbf{c}^{E}, \mathbf{e}, \varepsilon^{S})$ form distributes error components from single parameters to others, so that the exactness of the parameters decreases. Our proposed inverse scheme allows for an adjustment of given data sets to measured electric impedances and determines directly the parameters in the $(\mathbf{c}^{E}, \mathbf{e}, \varepsilon^{S})$ form . Even though, we can not proof, that our scheme identifies the physical parameters, we obtain for a selected frequency range a complete and consistent data set, which serves for further precise numerical computations. The proposed method will even be suited for the case, when no manufacturer's data are present, as long as one can provide appropriate initial guesses.

III. Physical Equations and Finite Element Discretization

The material law describing the piezoelectric effect in the linearized case of small mechanical deformations and electric fields, reads as

$$[\boldsymbol{\sigma}] = [\mathbf{c}^{E}][\mathbf{S}] - [\mathbf{e}]^{T}\mathbf{E} \quad (1)$$

$$\mathbf{D} = [\mathbf{e}][\mathbf{S}] + [\boldsymbol{\varepsilon}^{S}]\mathbf{E} \quad (2)$$

relating the mechanical stress tensor $[\boldsymbol{\sigma}]$ and the electrical displacement $\mathbf{D}$, respectively, to the mechanical strain tensor $[\mathbf{S}]$ and the electric field $\mathbf{E}$. Due to the symmetry of the mechanical tensors $[\boldsymbol{\sigma}]$ and $\mathbf{S}]$, we may rewrite them in Voigt notation as follows

$$\boldsymbol{\sigma} = \left(\sigma_{xx}\sigma_{yy}\sigma_{zz}\sigma_{yz}\sigma_{xz}\sigma_{xy}\right)^T \quad (3)$$

$$\mathbf{S} = \left(s_{xx}s_{yy}s_{zz}s_{yz}s_{xz}s_{xy}\right)^T . \quad (4)$$

For the electrostatic case, we may express $\mathbf{E}$ as the gradient of an electric potential ϕ

$$\mathbf{E} = -\boldsymbol{\nabla}\phi \,,$$

and $\mathbf{S}$ in terms of the mechanical displacements $\mathbf{u}$

$$\mathbf{S} = \mathcal{B}\mathbf{u} \,.$$

The first order differential operator $\mathcal{B}$ computes as

$$\mathcal{B} = \begin{pmatrix} \frac{\partial}{\partial x} & 0 & 0 \\ 0 & \frac{\partial}{\partial y} & 0 \\ 0 & 0 & \frac{\partial}{\partial z} \\ \frac{\partial}{\partial y} & \frac{\partial}{\partial x} & 0 \\ 0 & \frac{\partial}{\partial z} & \frac{\partial}{\partial y} \\ \frac{\partial}{\partial z} & 0 & \frac{\partial}{\partial x} \end{pmatrix}$$

i.e., the transposed of the divergence DIV of a dyadic. The material tensors $[\mathbf{c}^E]$, $[\boldsymbol{\varepsilon}^S]$, and $[\mathbf{e}]$, appearing in (1), (2) are the elasticity coefficients, the dielectric constants, and the piezoelectric coupling coefficients, respectively. According to the crystal structure and polarization of the piezoelectric material, these matrices show a certain symmetry and sparsity pattern (cf. [4]). For the 6mm crystal class we have, e.g.

$$[\mathbf{c}^E] = \begin{pmatrix} c_{11} & c_{12} & c_{13} & 0 & 0 & 0 \\ c_{12} & c_{11} & c_{13} & 0 & 0 & 0 \\ c_{13} & c_{13} & c_{33} & 0 & 0 & 0 \\ 0 & 0 & 0 & c_{44} & 0 & 0 \\ 0 & 0 & 0 & 0 & c_{44} & 0 \\ 0 & 0 & 0 & 0 & 0 & (c_{11}-c_{12})/2 \end{pmatrix}$$

$$[\mathbf{e}] = \begin{pmatrix} 0 & 0 & 0 & 0 & e_{15} & 0 \\ 0 & 0 & 0 & e_{15} & 0 & 0 \\ e_{31} & e_{31} & e_{33} & 0 & 0 & 0 \end{pmatrix} \quad (5)$$

$$[\boldsymbol{\varepsilon}^S] = \begin{pmatrix} \varepsilon_{11} & 0 & 0 \\ 0 & \varepsilon_{11} & 0 \\ 0 & 0 & \varepsilon_{33} \end{pmatrix} .$$

The mechanical behavior of piezoelectric materials is described by Newton's law

$$\mathrm{DIV}\boldsymbol{\sigma} = \mathcal{B}^T\boldsymbol{\sigma} = \rho\frac{\partial^2\mathbf{u}}{\partial t^2} \,, \quad (6)$$

where ρ denotes the density. Since these materials are insulating, i.e., do not contain free volume charges, the electric field is determined by

$$\boldsymbol{\nabla}\cdot\mathbf{D} = 0 \,. \quad (7)$$

Combining (1), (2), (6) and (7), we arrive at a system of four partial differential equations for $\mathbf{u}$ and ϕ, inside a piezoelectric body Ω

$$\rho\frac{\partial^2\mathbf{u}}{\partial t^2} - \mathcal{B}^T\left([\mathbf{c}^E]\mathcal{B}\mathbf{u} + [\mathbf{e}]^T\boldsymbol{\nabla}\phi\right) = 0 \quad \text{in } \Omega \quad (8)$$

$$-\boldsymbol{\nabla}\cdot\left([\mathbf{e}]\mathcal{B}\mathbf{u} - [\boldsymbol{\varepsilon}^S]\boldsymbol{\nabla}\phi\right) = 0 \quad \text{in } \Omega \,. \quad (9)$$

Considering the experimental setting of vanishing normal stress at the boundary, and two electrodes being applied at opposite positions Γ_g and Γ_e, one of them loaded by a prescribed electric potential ϕ^e, we arrive at the boundary conditions

$$\begin{aligned} \boldsymbol{\sigma}_{\mathrm{n}} &= 0 && \text{on } \partial\Omega \\ \phi &= 0 && \text{on } \Gamma_g \\ \phi &= \phi^e && \text{on } \Gamma_e \\ \mathbf{D}\cdot\mathbf{n} &= 0 && \text{on } \partial\Omega \setminus (\Gamma_g \cup \Gamma_e) \,. \end{aligned} \quad (10)$$

Therewith, the variational formulation for the case of a harmonic excitation reads as

$$\int_\Omega \Big(-\rho\omega^2\hat{\mathbf{u}}^T\mathbf{v} + (\mathcal{B}\hat{\mathbf{u}})^T[\mathbf{c}^E](\mathcal{B}\mathbf{v}) + (\boldsymbol{\nabla}\hat{\phi})^T[\mathbf{e}](\mathcal{B}\mathbf{v}) \Big)\,\mathrm{d}\Omega = 0 \quad (11)$$

$$\int_\Omega \Big((\boldsymbol{\nabla}\psi)^T[\mathbf{e}](\mathcal{B}\hat{\mathbf{u}}) - (\boldsymbol{\nabla}\hat{\phi})^T[\boldsymbol{\varepsilon}](\boldsymbol{\nabla}\psi) \Big)\,\mathrm{d}\Omega = 0 \quad (12)$$

with ω the angular frequency and $\mathbf{v}$, ψ appropriate test functions.

The application of a finite element discretization scheme to these equations ends up with a linear system of equations, which can be summarized as [11]

$$\begin{pmatrix} -\omega^2\mathbf{M}_{uu} + \mathbf{K}_{uu} & \mathbf{K}_{u\phi} \\ \mathbf{K}_{u\phi}^T & -\mathbf{K}_{\phi\phi} \end{pmatrix} \begin{pmatrix} \underline{\hat{u}} \\ \underline{\hat{\phi}} \end{pmatrix} = \begin{pmatrix} 0 \\ 0 \end{pmatrix} . \quad (13)$$

Herein $\mathbf{K}_{uu}$, and $\mathbf{M}_{uu}$ denote the mechanical stiffness, and mass matrix, respectively, $\mathbf{K}_{\phi\phi}$ and $\mathbf{K}_{u\phi}$ the dielectric stiffness- and the piezoelectric coupling matrix, $\underline{\hat{u}}$ the nodal vector of displacement and $\underline{\hat{\phi}}$ the nodal vector of scalar electric potential. We want to note, the we allow for our material tensors to have complex entries, in order to model the damping behavior, namely mechanical relaxation, imperfect piezoelectric energy conversion and dielectric dissipation (see, e.g. [12]), of piezoelectric materials.

IV. Parameter Identification Algorithm

The main task we are concerned with is to adapt all occurring material parameters in the piezoelectric equations in such a way, that simulated results coincide with those received from measurements, namely the electric impedance. In an abstract setting this can be formulated with the so called parameter-to-solution map $\hat{\mathcal{F}}$

$$\hat{\mathcal{F}} : \mathcal{C}^{n_{\mathrm{par}}} \to \mathcal{C}^{n_{\mathrm{freq}}}, \quad \hat{\mathcal{F}}(\mathbf{p}) = \hat{\mathbf{y}} \quad (14)$$

mapping from the set of $n_{\rm par}$ complex valued parameters $\mathbf{p} = (c_{11}^E, c_{12}^E, c_{13}^E, c_{33}^E, c_{44}^E, e_{15}, e_{31}, e_{33}, \varepsilon_{11}^S, \varepsilon_{33}^S)$ or subsets of it to the set of measuremets $\hat{\mathbf{y}}$ taken at $n_{\rm freq}$ different frequencies. (To stress that the computations are performed in frequency domain all expressions are marked by $\hat{\cdot}$.) The measurements may either contain measured impedances or mechanical displacements or a combination of them at different frequencies $\omega_i,\ i = 1, ..., n_{freq}$.

From the FE solution of the piezoelectric PDEs we obtain directly the mechanical displacement $\hat{\mathbf{u}}$ and electric potential $\hat{\phi}$ at all FE nodes and by a post-processing step the electric impedance $\hat{Z}(\omega_i)$

$$\begin{aligned} \hat{q}^e(\omega_i) &= \int_{\Gamma_e} \mathbf{n}^T \Big(-[\mathbf{e}]\mathcal{B}^T \hat{\mathbf{u}}(\omega_i) + [\boldsymbol{\varepsilon}^S]\boldsymbol{\nabla}\hat{\phi}(\omega_i) \Big)\, d\Gamma_e \\ \hat{Z}(\omega_i) &= \frac{\phi^e}{j\omega_i \hat{q}^e(\omega_i)}, \quad i = 1, ..., n_{\rm freq}, \end{aligned} \tag{15}$$

where $\hat{q}^e(\omega_i)$ denotes the computed surface charges on the loaded electrode.

Eventhough, solving (13) is a linear problem, the operator $\hat{\mathcal{F}}$ is strongly nonlinear. Furtheron, it is not guaranteed that each parameter will depend in a stable manner on the measurements and additionally the right-hand side in (14) is contaminated with data noise, which makes (14) a typical ill-posed problem. Its solution requires appropriate regularization methods, from which we have investigated a regularizing Newton method and a regularizing modified Landweber iteration. Both methods are minimizing the norm of the residual $||\hat{\mathcal{F}}(\mathbf{p}) - \hat{\mathbf{y}}||$ until a lower bound of $\tau\delta$ with $\tau > 1$ is reached. Here, the variable δ denotes a measure of the quality of the measurements, being more precise $||\hat{\mathbf{y}} - \hat{\mathbf{y}}^\delta|| \le \delta$ where $\hat{\mathbf{y}}$ denotes exact data for this model and $\hat{\mathbf{y}}^\delta$ contains a certain noise level resulting from inexactness in the measurements. Doing so the early stopping of the iterations avoids amplification of the noise components in the computed data. In both methods, we need to compute the Jacobian $\hat{\mathcal{F}}'$. Forming for a parameter increment $d\mathbf{p}$ the difference $\hat{\mathcal{F}}(\mathbf{p} + d\mathbf{p}) - \hat{\mathcal{F}}(\mathbf{p})$, one obtains $\hat{\mathcal{F}}(\mathbf{p})'[d\mathbf{p}] = d\hat{\mathbf{y}}$, where in discrete form $\underline{d\hat{y}} = (\underline{d\hat{u}}, \underline{d\hat{\phi}})$ and $\underline{d\hat{u}}$ and $\underline{d\hat{\phi}}$ are solutions of the following system

$$\begin{pmatrix} \mathbf{K}_{uu} & \mathbf{K}_{u\phi} \\ \mathbf{K}_{u\phi}^T & -\mathbf{K}_{\phi\phi} \end{pmatrix} \begin{pmatrix} \underline{d\hat{u}} \\ \underline{d\hat{\phi}} \end{pmatrix} = \begin{pmatrix} d\mathbf{K}_{uu} & d\mathbf{K}_{u\phi} \\ d\mathbf{K}_{u\phi}^T & -d\mathbf{K}_{\phi\phi} \end{pmatrix} \begin{pmatrix} \underline{\hat{u}} \\ \underline{\hat{\phi}} \end{pmatrix}.$$

Here, the matrix on the RHS is obtained by substituting the parameters $\mathbf{p}$ by $d\mathbf{p}$ in the bilinear forms of (11) and applying the FE assembly.

1) Inexact Newton Iteration: In algorithmical design, the application of the inexact Newton iteration (see, e.g., [13], [14], [15]) results in the following algorithm.

CHOOSE $\mathbf{p}^0$;
SET $k = 0$;
WHILE $\|\hat{\mathbf{y}} - \hat{\mathcal{F}}(\mathbf{p}^k)\| \ge \tau\delta$
  SET $i = 0$;
  SET $\mathbf{s}_0^{k,\delta} = 0$;
  WHILE $||\hat{\mathbf{y}}^\delta - \hat{\mathcal{F}}(\mathbf{p}^{k,\delta}) - \hat{\mathcal{F}}'(\mathbf{p}^{k,\delta})[\mathbf{s}_i^{k,\delta}]||$
    $\ge \eta_k ||\hat{\mathbf{y}}^\delta - \hat{\mathcal{F}}(\mathbf{p}^k)||$ (*)
    $\mathbf{s}_{i+1}^{k,\delta} = \Phi(\hat{\mathcal{F}}'(\mathbf{p}^{k,\delta}), \hat{\mathbf{y}}^\delta - \hat{\mathcal{F}}(\mathbf{p}^{k,\delta}), \mathbf{s}_i^{k,\delta})$;
    $i = i + 1$;
  $\mathbf{p}^{k+1,\delta} = \mathbf{p}^{k,\delta} + \theta \mathbf{s}_i^{k,\delta}$;
  $k = k + 1$;

Here, the mapping Φ stands representatively for a linear iterative regularizing method, e.g. Landweber, $\nu-$ or the conjugate gradient method (see again [16], [14], [13]) are possible choices. Mainly, our choice for these iterative methods bases on the fact, that the regularization parameter, here the number of iteration steps, can easily be determined a posteriori by the discrepancy principle in (*). The steering parameter $0 < \eta_k \le \bar{\eta} < 1$ influences the trade of between convergence and stability of the inner method. For optimal choices of η_k see [17]. Applying additionally linesearch strategies steering the parameter $\theta > 0$ improves convergence and prevents divergence. The initial guess $\mathbf{p}^0$ of unknown materials will be accomplished using the methods prescribed in the standards [4], [5] or taking over parameters from well known materials with similar physical properties.

2) Modified Landweber Iteration: Alternatively one can implement a nonlinear iterative regularizing method, where the most simple one is nonlinear Landweber's iteration. Here during the fixed-point iterations an adjoint problem applied to the residual will be solved, see e.g. [16] or [18]

$$\mathbf{p}^{k+1,\delta} = \mathbf{p}^{k,\delta} + w^{k,\delta} \hat{\mathcal{F}}'(\mathbf{p}^{k,\delta})^*(\hat{\mathbf{y}}^\delta - \hat{\mathcal{F}}(\mathbf{p}^{k,\delta})), \quad k = 1, ... \tag{16}$$

with $||w^{k,\delta}\hat{\mathcal{F}}'(\mathbf{p}^{k,\delta})|| \le 1||$. The operator $\hat{\mathcal{F}}'(\mathbf{p}^{k,\delta})^* = \hat{\mathcal{F}}'(\mathbf{p}^{k,\delta})^H$ (complex conjugate) denotes the adjoint of $\hat{\mathcal{F}}'(\mathbf{p}^{k,\delta})$. The special choices of $w^{k,\delta}$, e.g.

$$w^{k,\delta} := \frac{||\hat{\mathcal{F}}'(\mathbf{p}^{k,\delta})^*(\hat{\mathbf{y}}^\delta - \hat{\mathcal{F}}(\mathbf{p}^{k,\delta}))||^2}{||\hat{\mathcal{F}}'(\mathbf{p}^{k,\delta})\hat{\mathcal{F}}'(\mathbf{p}^{k,\delta})^*(\hat{\mathbf{y}}^\delta - \hat{\mathcal{F}}(\mathbf{p}^{k,\delta}))||^2} \tag{17}$$

or

$$w^{k,\delta} := \frac{||\hat{\mathbf{y}}^\delta - \hat{\mathcal{F}}(\mathbf{p}^{k,\delta})||^2}{||\hat{\mathcal{F}}'(\mathbf{p}^{k,\delta})^*(\hat{\mathbf{y}}^\delta - \hat{\mathcal{F}}(\mathbf{p}^{k,\delta}))||^2} \tag{18}$$

transforms the Landweber iteration into a steepest descent or minimal error method which remarkably speed up the convergence compared to the classical Landweber iteration.

A crucial point for the successful identification is an appropriate scaling of both parameters and measurements. Thus, within the identification methods the parameters are equilibrated, i.e. $\mathbf{p} = \xi * \mathbf{p}$ where $\xi \approx diag(1/p_1, ...1/p_{N_{\rm par}})$. To compare the measured and computed electric impedances, denoted by $\hat{\mathbf{y}}_i^\delta$ and $\hat{\mathcal{F}}_i(\mathbf{p})$, at different frequencies, we evaluate the following logarithmic norm

$$||\hat{\mathbf{y}} - \hat{\mathcal{F}}(\mathbf{p})||_w := \sum_{i=1}^{N_{\rm freq}} \frac{|\log(\hat{\mathbf{y}}_i^\delta) - \log(\hat{\mathcal{F}}_i(\mathbf{p}))|^2)}{|\log(\hat{\mathbf{y}}_i^\delta)|^2}.$$

Therewith, we consider the different orders of magnitudes between impedance measurements at various frequencies.

TABLE I
COMPUTED CONFIDENCE INTERVALS OF DIFFERENT MODE SHAPES

	c_{11}^E	c_{33}^E	c_{12}^E	c_{13}^E	c_{44}^E
Radial	0.096	0.12	0.2	0.05	5.8e+05
Thickness	1.8	2.1	1.1e+06	1.7	1.6e+05
Longitudinal	0.14	0.17	0.30	0.086	1.86e+06
Transversal	1.96	4.0	28.9	7.7	3.3e+03
Shear	0.014	0.06	0.027	0.033	0.016

	e_{15}	e_{31}	e_{33}	ε_{11}^S	ε_{33}^S
Radial	3.0e+06	3.82	1.22	5.47e+7	1.84
Thickness	2.8e+05	2.6e+03	3.3	3.9e+05	2.0
Longitudinal	9.09e+06	12.03	3.7	9.48e+07	6.03
Transversal	1.61e+06	1.19e+03	29.0	1.34e+07	16.1
Shear	0.68	73.5	11.7	33.3	1.28

V. SENSITIVITY ANALYSIS

Since not all material parameters show a visible impact on the solution of the piezoelectric PDEs, we like to understand, which of them dominate in the different types of probes. These are differing in e.g. geometry, polarization and range of excitation frequency. In the following we interprete the linearization $\hat{\mathcal{F}}'$ of the highly nonlinear relation between parameters and observations $\hat{\mathcal{F}}(\mathbf{p}) = \hat{\mathbf{y}}$. Confidence intervals of the identified parameters can be estimated by evaluating diagonal entries of the inverse of the information matrix

$$\mathbf{C} = \sum_{i=1}^{n_{\text{freq}}} \left(\hat{\mathcal{F}}'(\mathbf{p}, \omega_i)^H \hat{\mathcal{F}}'(\mathbf{p}, \omega_i) \right)^{-1} \in \mathcal{C}^{n_{\text{par}} \times n_{\text{par}}}. \quad (19)$$

The sensitivity of each parameter is related to a diagonal entry in this matrix $\mathbf{C}$ and one can say that the probability that

$$|p_i^{\text{exact}} - p_i^{\text{computed}}| \leq \sqrt{C_{ii} \chi^2_{n_{\text{par}}}(1-\alpha)}, \; i = 1, ..., n_{\text{par}} \quad (20)$$

is larger than $(1-\alpha)$, where $\chi^2_{n_{\text{par}}}(1-\alpha)$ denotes the $(1-\alpha)$ quantile of the $\chi^2_{n_{\text{par}}}$ probability distribution. Thus, the smaller the term on the RHS in (20), the more reliable the identified parameter and the higher its influence on the transducers behavior can be considered. Table I contains upper bounds of the sizes of the confidence intervals using $\alpha = 0.01$ for transducers working in radial, thickness, longitudinal, transversal and thickness shear mode.

Setting a threshold of approximately 10, the set of parameters of each mode disintegrates into two subsets of parameters. Parameters, whose confidence interval are sufficiently small, are reliable, the others are far away from identifiability. In the latter case results from identifications of other modes have to be called on. Due to the dependency of the computed confidence intervals on the location and number of selected frequencies their values can only be compared qualitatively, but not quantitatively. An appropriate choice of measurement locations providing the highest amount of information for the identification process can be achieved by means of optimal experiment design and is discussed in [19].

A Remark concerning the shear mode: In the frequency range, where we see the first mode of the shear vibration, higher modes of the thickness vibration are present (see Figure 5). Performing measurements at such a frequency interval allows to identify even parameters, dominating in thickness mode.

VI. COMPUTATIONAL ASPECTS

Concerning the forward problem, the piezoelectric samples operating at radial, thickness and longitudinal mode are modeled as rotationally symmetric problems. The others, the thin plates vibrating in transversal and shear modes need full three dimensional meshes. Approximately 250 2nd order quadrilateral elements are used for the rotationally symmetric and 320 2nd order hexahedron elements for the 3D case. The sparse direct solver PARDISO, an efficient software for solving large sparse symmetric and unsymmetric linear systems of equations, is employed to solve the arising algebraic system of equations [20]. Solving the inverse problem, namely the inexact Newton (e.g. with the ν - methods as inner method) or modified Landweber methods comes with a price since here the forward problem needs to be solved repeatedly. Figure 1 compares the two different methods fitting the longitudinal mode of Pz36, and displays the decrease of the residuals (for the fitting results, see Fig. 8). Here, all real and imaginary parts of the parameters are determined simultaneously. Both methods are run until the norm of the residual ($\|\hat{\mathbf{y}} - \hat{\mathcal{F}}(\mathbf{p})\|$) falls below 5.0×10^{-4}. The computing times are 17.5 minutes for the Newton-ν-methods (8 steps) and around 22.4 minutes for the modified Landweber's iteration (10 steps) on a 64 bit Intel(R) Pentium(R) D CPU 2.80GHz machine. In case, that the initial guess is not as suitable as in this case, it is advisable to start the inverse calculation with less input, i.e. a viewer number of measurements until one reaches a certain accuracy. Then, we restart the program evaluating an increasing number of impedance measurements and improve the exactness of the results.

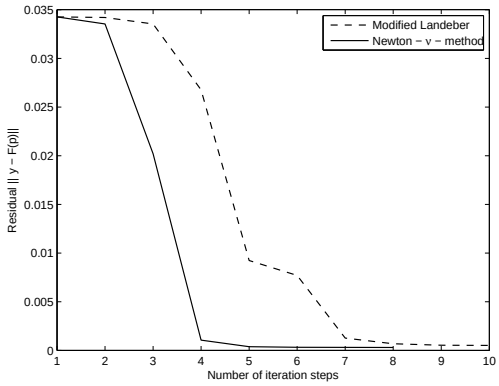

Fig. 1. Development of residual of the methods proposed during the parameter identification at the longitudinal mode, Pz36

VII. IDENTIFICATION RESULTS

In this section we will present results of our proposed method applied to two different piezoelectric materials. On the one hand, we have chosen a well known material, where the manufacturer provides a complete set of material parameters (Pz26, Ferroperm) and on the other hand a recently developed material (Pz36, Ferroperm), for which until now, no material data are available. For the first material, Pz26, we use the

manufacturer's data as starting values for our developed inverse scheme and determine real and complex valued material parameters appropriate for precise FE simulations. For the second material, we show how one can obtain a consistent parameter set, even if one starts more or less from the scratch.

A. Pz-26

The manufacturer's data for this material, which is a hard PZT with low ageing rates and low loss [21], are given in Table II. For our investigations, we used the three piezoelectric

TABLE II
PUBLISHED MATERIAL PARAMETERS OF PZ26, FERROPERM

$\mathbf{c}_{11}^E$	$\mathbf{c}_{33}^E$	$\mathbf{c}_{12}^E$	$\mathbf{c}_{13}^E$	$\mathbf{c}_{44}^E$
1.68e+11	1.23e+11	1.10e+11	9.99e+10	3.01e+10

$\mathbf{e}_{15}$	$\mathbf{e}_{31}$	$\mathbf{e}_{33}$	ε_{11}^S	ε_{33}^S
9.86	-2.80	14.7	7.33e-09	6.2e-09

samples as listed in Tab.III.

TABLE III
GEOMETRY OF THE USED PZ26 SAMPLES

Name	Geometry
Disc 1	radius $= 8$ mm, thickness $= 1$ mm
Disc 2	radius $= 8$ mm, thickness $= 4$ mm
Bar	length $= 20$ mm, width $= 5$ mm, height $= 1$ mm

1) Radial Mode: We start our investigation with disc 1, which operates at its radial mode. We use the manufacturer's data as starting parameters and apply our inverse scheme in order to fit the simulated impedance curve to the measured one. Figure 2 displays the three curves, namely the measured impedance and the two simulated impedances computed with the manufacturer's as well as fitted material parameters. As can be seen, the material parameters obtained by our inverse scheme provides improvements concerning the location of the resonance frequency and appropriate damping. Results of the identification concerning the real valued parameters are listed in Table IV. For the initial guesses of the imaginary part of the

TABLE IV
RESULTS OF FITTING AT RADIAL MODE, REAL PARTS, PZ26

$\mathbf{c}_{11}^E$	$\mathbf{c}_{33}^E$	$\mathbf{c}_{12}^E$	$\mathbf{c}_{13}^E$	$\mathbf{c}_{44}^E$
1.62e+11	1.26e+11	1.10e+11	9.82e+10	3.00e+10

$\mathbf{e}_{15}$	$\mathbf{e}_{31}$	$\mathbf{e}_{33}$	ε_{11}^S	ε_{33}^S
9.86	-2.82	14.26	7.33e-09	6.32e-09

complex valued material parameters, we have assumed a value being approximately one per mill from its real part. This can be motivated considering the usual Rayleigh damping as a special case of complex valued parameters (see, e.g., [22], [11]). If one has found appropriate values for the Rayleigh damping coefficients $\alpha(\omega)$ and $\beta(\omega)$, complex valued parameters can be computed via

$$[\tilde{\mathbf{c}}^E] := \frac{1+j\beta_0}{1-j\alpha_0}[\mathbf{c}^E] \qquad [\tilde{\mathbf{e}}] := \frac{1}{1-j\alpha_0}[\mathbf{e}]$$
$$[\tilde{\boldsymbol{\varepsilon}}] := \frac{1}{1-j\alpha_0}[\boldsymbol{\varepsilon}]\,,$$

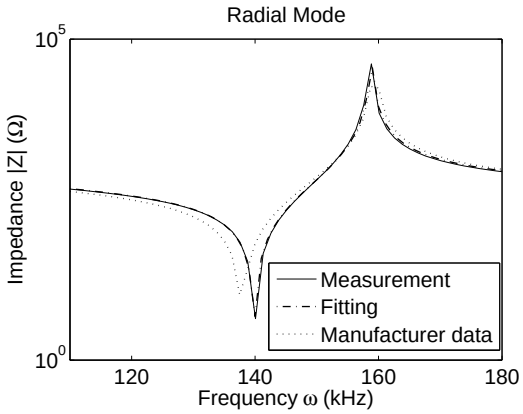

Fig. 2. Radial mode: measured and simulated impedance curves, Pz26

where $\alpha(\omega) = \alpha_0\omega$ and $\beta(\omega) = \beta_0/\omega$. The values in Tab.

TABLE V
IMAGINARY PARTS, INITIAL GUESS AND IDENTIFIED PARAMETERS, RADIAL MODE, PZ26

$\mathbf{c}_{11}^E$	$\mathbf{c}_{33}^E$	$\mathbf{c}_{12}^E$	$\mathbf{c}_{13}^E$	$\mathbf{c}_{44}^E$
1.68e+9	1.23e+9	1.10e+9	9.99e+8	3.01e+8
7.07e+07	4.48e+08	5.33e+07	1.85e+08	1.13e+08

$\mathbf{e}_{15}$	$\mathbf{e}_{31}$	$\mathbf{e}_{33}$	ε_{11}^S	ε_{33}^S
0.098	-0.028	0.14	7.3e-11	6.2e-11
0.1001	-0.0286	0.135	7.34-11	6.52e-11

V reveal that in particular for the mechanical parts the initial damping was too strong. Figure 3 shows the measured and simulated phase of the electric impedance. Again, using the

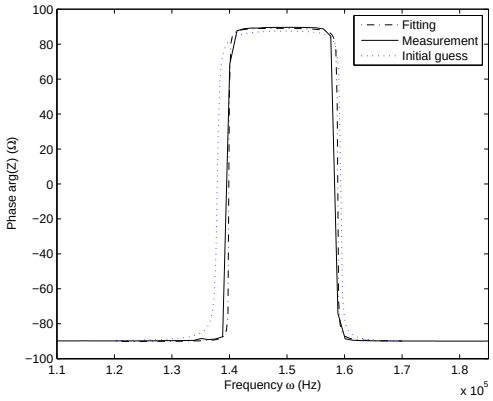

Fig. 3. Phase of the electric impedance at radial mode, Pz26

fitted material parameters, we achieve a good approximation of the measured impedance curve.

2) Combined Radial and Thickness Mode: Of great interest for a simulation based material parameter identification are such geometries, where different modes occur in a similar frequency range and allow to adapt for a larger set of parameters. This is exemplarily done with disc 2, where the radial mode is at 140 kHz and the thickness mode at 510 kHz. Now, we

use in our inverse scheme already the data set obtained by our first fitting procedure. The results can be seen in Fig. 4, where we again display the measured and simulated (once with the manufacturer's and once with the fitted material parameters) impedance curves. Since the impedance curve shows quite

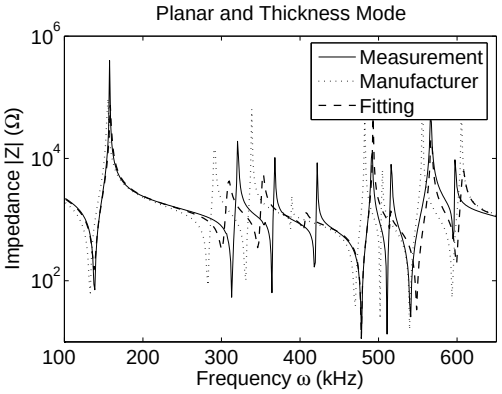

Fig. 4. Simultaneous fitting of radial and thickness mode, Pz26

a lot of piezoelectric coupling modes, we can not expect to obtain a fitting as in the previous case. Table VI lists the real and imaginary material parameters as obtained by the inverse scheme.

TABLE VI
RESULTS OF SIMULTANEOUS FITTING AT THICKNESS AND RADIAL MODE, REAL AND IMAGINARY PARTS, PZ26

Real parts

$\mathbf{c}_{11}^E$	$\mathbf{c}_{33}^E$	$\mathbf{c}_{12}^E$	$\mathbf{c}_{13}^E$	$\mathbf{c}_{44}^E$
1.682e+11	1.25e+11	9.84e+10	9.47e+10	2.92e+10

$\mathbf{e}_{15}$	$\mathbf{e}_{31}$	$\mathbf{e}_{33}$	ε_{11}^S	ε_{33}^S
10.33	-2.84	14.62	7.18-09	6.28e-09

Imaginary parts

$\mathbf{c}_{11}^E$	$\mathbf{c}_{33}^E$	$\mathbf{c}_{12}^E$	$\mathbf{c}_{13}^E$	$\mathbf{c}_{44}^E$
6.24e+07	2.50e+08	5.33e+07	1.33e+08	2.27+07

$\mathbf{e}_{15}$	$\mathbf{e}_{31}$	$\mathbf{e}_{33}$	ε_{11}^S	ε_{33}^S
0.09966	-0.0287	0.13	1.25e-10	2.1e-10

3) Thickness Shear Mode: The largest discrepancy between manufacturer's data and measurements are noticeable for the shear mode. Figure 5 compares the measured and simulated impedance curves, and in Tab. VII we list the real and imaginary parts of the fitted material parameters.

As described in Sec. V, we have quite different confidence intervals for the different piezoelectric modes. Providing a consistent data set, we choose the material parameters out of our fitting results according to the confidence intervals. Table VIII provides this consistent data set for our first piezoelectric material under investigation. Since damping is a really frequency depended phenomena, no consistent data set will be provided here. Using now this set of material parameters and performing FE simulations of the electric impedance of our three samples, results still in the good comparison to the measured ones.

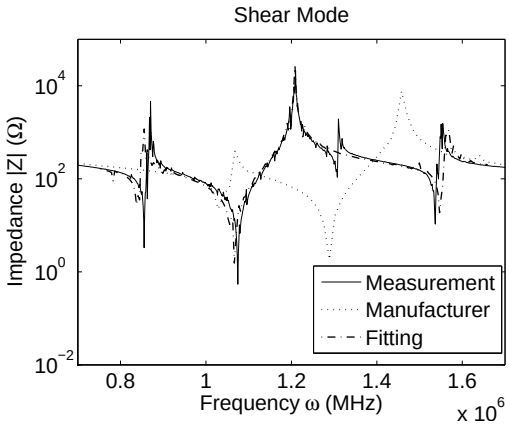

Fig. 5. Fitting of shear mode, Pz26

TABLE VII
FITTING AT SHEAR MODE, REAL AND IMAGINARY MATERIAL PARAMETERS, PZ26

Real parts

$\mathbf{c}_{11}^E$	$\mathbf{c}_{33}^E$	$\mathbf{c}_{12}^E$	$\mathbf{c}_{13}^E$	$\mathbf{c}_{44}^E$
1.31e+11	1.11e+11	1.06e+11	9.18e+10	2.12e+10

$\mathbf{e}_{15}$	$\mathbf{e}_{31}$	$\mathbf{e}_{33}$	ε_{11}^S	ε_{33}^S
8.18	-2.38	14.05	7.19e-09	6.41e-09

Imaginary parts

$\mathbf{c}_{11}^E$	$\mathbf{c}_{33}^E$	$\mathbf{c}_{12}^E$	$\mathbf{c}_{13}^E$	$\mathbf{c}_{44}^E$
1.03e+09	8.15e+08	1.06e+09	9.81e+08	2.4e+08

$\mathbf{e}_{15}$	$\mathbf{e}_{31}$	$\mathbf{e}_{33}$	ε_{11}^S	ε_{33}^S
0.102	-0.028	0.13	7.33e-11	6.48e-11

VIII. PZ-36

For our second practical application, we have chosen Pz36, which is a new type of piezoceramic material with very low acoustic impedance [21]. Until now, no manufacturer data are published. The samples listed in Tab. IX have been used for our investigations. To obtain starting material parameters for our inverse scheme, we have measured the electric impedances and have extracted the parameters according to the IEEE standard [4]. Since the used samples do not fulfill the IEEE standard, we can not expect to obtain good starting values. However, this is not our intention, since we also want to demonstrate, that our developed inverse scheme performs well, even for such starting parameters. The values of this procedure are listed in Tab. X.

TABLE VIII
CONSISTENT DATA SET FOR PZ26 FROM FEM BASED FITTING, REAL PARTS

$\mathbf{c}_{11}^E$	$\mathbf{c}_{33}^E$	$\mathbf{c}_{12}^E$	$\mathbf{c}_{13}^E$	$\mathbf{c}_{44}^E$
1.31e+11	1.25e+11	1.1e+11	9.7e+10	2.12e+10

$\mathbf{e}_{15}$	$\mathbf{e}_{31}$	$\mathbf{e}_{33}$	ε_{11}^S	ε_{33}^S
8.18	-2.82	14.26	7.19e-09	6.33e-09

TABLE IX
GEOMETRY OF THE USED PZ36 SAMPLES

Name	Geometry
Disc	radius $= 8$ mm, thickness $= 1$ mm
Cylinder	radius $= 2.5$ mm, length $= 18$ mm
Bar	length $= 25$ mm, width $= 4$ mm, height $= 1$ mm

TABLE X
MATERIAL PARAMETERS OF PZ36, AS EXTRACTED FROM IMPEDANCE MEASUREMENTS ACCORDING TO IEEE STANDARD

$\mathbf{c}_{11}^E$	$\mathbf{c}_{33}^E$	$\mathbf{c}_{12}^E$	$\mathbf{c}_{13}^E$	$\mathbf{c}_{44}^E$
4.49e+10	3.46e+10	7.21e+11	7.29e+10	1.32e+10
$\mathbf{e}_{15}$	$\mathbf{e}_{31}$	$\mathbf{e}_{33}$	ε_{11}^S	ε_{33}^S
2.56	-0.41	6.57	4.16e-09	5.59e-09

A. Radial Mode

We start our procedure with our piezoelectric disc (see Tab. IX) and investigate in the radial mode. Figure 6 displays the measured and computed electric impedances. Due to the clear

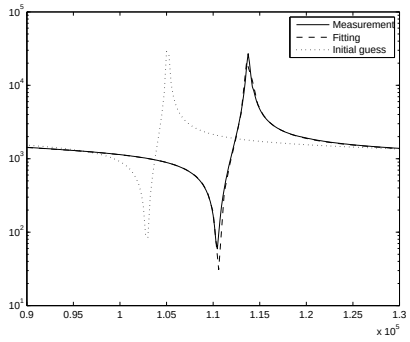

Fig. 6. Fitting at radial mode, Pz36

radial mode of this sample, we achieve an optimal fitting. The obtained material parameters are shown in Tab. XI.

TABLE XI
RESULTS RADIAL MODE, REAL AND IMAGINARY PARTS, PZ36

Real parts

$\mathbf{c}_{11}^E$	$\mathbf{c}_{33}^E$	$\mathbf{c}_{12}^E$	$\mathbf{c}_{13}^E$	$\mathbf{c}_{44}^E$
5.59e+10	3.41e+10	1.029e+10	1.53e+10	1.13e+10
$\mathbf{e}_{15}$	$\mathbf{e}_{31}$	$\mathbf{e}_{33}$	ε_{11}^S	ε_{33}^S
2.56	-0.0409	6.96	4.659e-09	3.743e-09

Imaginary parts

$\mathbf{c}_{11}^E$	$\mathbf{c}_{33}^E$	$\mathbf{c}_{12}^E$	$\mathbf{c}_{13}^E$	$\mathbf{c}_{44}^E$
3.15e+08	3.03e+08	9.26e+07	2.15e+08	1.13e+08
$\mathbf{e}_{15}$	$\mathbf{e}_{31}$	$\mathbf{e}_{33}$	ε_{11}^S	ε_{33}^S
0.0256	-0.00041	0.067	4.66e-11	3.815e-11

B. Thickness Mode

The second fitting is performed on the same piezoelectric disc by investigating into the thickness mode and using as starting values the one obtained by the radial mode (see Tab. XI). As can be seen from Fig. 7, this mode is disturbed by a lot of smaller ones, which is mainly due to the geometry of the sample. However, our inverse scheme still achieves a good result. The material parameters, as obtained by our scheme,

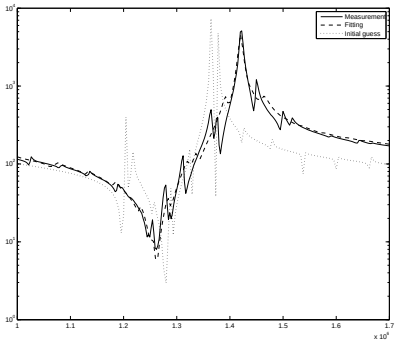

Fig. 7. Fitting at thickness mode, Pz36

are listed in Tab. XII.

TABLE XII
RESULTS THICKNESS MODE, PZ36

Real parts

$\mathbf{c}_{11}^E$	$\mathbf{c}_{33}^E$	$\mathbf{c}_{12}^E$	$\mathbf{c}_{13}^E$	$\mathbf{c}_{44}^E$
6.02e+10	3.45e+10	1.02e+10	1.51e+10	1.12e+10
$\mathbf{e}_{15}$	$\mathbf{e}_{31}$	$\mathbf{e}_{33}$	ε_{11}^S	ε_{33}^S
2.55	-0.0409	6.54	4.65e-09	3.69e-09,

Imaginary parts

$\mathbf{c}_{11}^E$	$\mathbf{c}_{33}^E$	$\mathbf{c}_{12}^E$	$\mathbf{c}_{13}^E$	$\mathbf{c}_{44}^E$
7.24e+08	1.82e+08	1.03e+08	1.49e+08	1.13e+08
$\mathbf{e}_{15}$	$\mathbf{e}_{31}$	$\mathbf{e}_{33}$	ε_{11}^S	ε_{33}^S
0.025	-0.000409	0.0407	4.665e-11	5.35293e-11,

C. Longitudinal Mode

To perform the fitting for the longitudinal mode, we use the cylindrical sample as listed in Tab. IX. Figure 8 shows

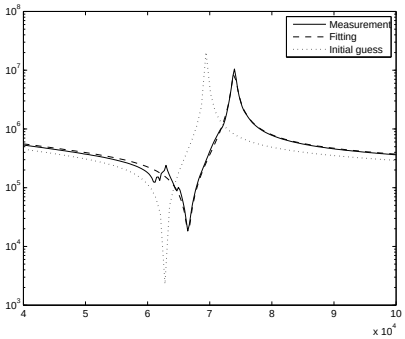

Fig. 8. Fitting at longitudinal mode, Pz36

the electric impedances, and Tab. XIII displays the obtained material parameters.

TABLE XIII
RESULTS LONGITUDINAL MODE, PZ36

Real values

$\mathbf{c}_{11}^E$	$\mathbf{c}_{33}^E$	$\mathbf{c}_{12}^E$	$\mathbf{c}_{13}^E$	$\mathbf{c}_{44}^E$
5.68e+10	3.77e+10	1.03e+10	1.45e+10	1.13e+10

$\mathbf{e}_{15}$	$\mathbf{e}_{31}$	$\mathbf{e}_{33}$	ε_{11}^S	ε_{33}^S
2.56	-0.041	6.42	4.65e-09	4.58e-09

Imaginary values

$\mathbf{c}_{11}^E$	$\mathbf{c}_{33}^E$	$\mathbf{c}_{12}^E$	$\mathbf{c}_{13}^E$	$\mathbf{c}_{44}^E$
5.62e+08	3.52e+08	1.03e+08	1.48e+08	1.13e+08

$\mathbf{e}_{15}$	$\mathbf{e}_{31}$	$\mathbf{e}_{33}$	ε_{11}^S	ε_{33}^S
0.0256	-0.00041	0.055	4.66e-11	5.02e-11

D. Shear Mode

The last sample used for determining the material parameters for Pz36, is operating at its shear mode. Figure 9 displays electric impedances as obtained from the measurement and simulations. The fitted material parameters computed by our

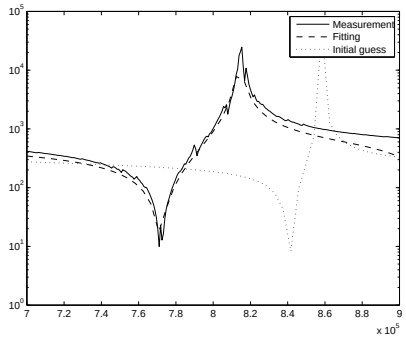

Fig. 9. Fitting at shear mode, Pz36

inverse scheme are listed in Tab. XIV.

TABLE XIV
RESULTS SHEAR MODE, PZ36

Real parts

$\mathbf{c}_{11}^E$	$\mathbf{c}_{33}^E$	$\mathbf{c}_{12}^E$	$\mathbf{c}_{13}^E$	$\mathbf{c}_{44}^E$
5.64e+10	3.48e+10	1.03e+10	1.49e+10	1.13e+10

$\mathbf{e}_{15}$	$\mathbf{e}_{31}$	$\mathbf{e}_{33}$	ε_{11}^S	ε_{33}^S
2.78	-0.041	6.87	4.66e-09	3.55e-09

Imaginary parts

$\mathbf{c}_{11}^E$	$\mathbf{c}_{33}^E$	$\mathbf{c}_{12}^E$	$\mathbf{c}_{13}^E$	$\mathbf{c}_{44}^E$
5.44e+08	3.47e+08	1.03e+08	1.50e+08	4.04e+07

$\mathbf{e}_{15}$	$\mathbf{e}_{31}$	$\mathbf{e}_{33}$	ε_{11}^S	ε_{33}^S
0.023	-0.00041	0.068	4.66e-11	3.92e-11

E. Thickness Mode, verification of identification results

Applying the proposed simulation based inversion scheme to a set of differently shaped samples and considering again those parameters with small confidence intervals provides a rather consistent, except frequency dependency, set of piezoelectric material parameters, see Table XV. In order to show the improvement in the data set, we apply the identified material parameters to a sample, which has not been considered so far, namely a radial disc working in thickness mode with a thickness of $4\,\mathrm{mm}$ and diameter of $16\,\mathrm{mm}$. Figure 10 shows the simulated impedance curve which gives a reasonable approximation to the measured one. Still, and

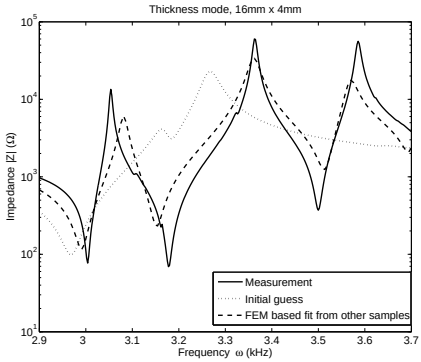

Fig. 10. Computed impedance of a not identified specimen using the identified parameters compared to the simulation with the initial guess and measurement

TABLE XV
CONSISTENT DATA SET FOR PZ36 FROM FEM BASED FITTING, REAL PARTS

$\mathbf{c}_{11}^E$	$\mathbf{c}_{33}^E$	$\mathbf{c}_{12}^E$	$\mathbf{c}_{13}^E$	$\mathbf{c}_{44}^E$
5.61e+10	3.48e+10	1.06e+10	1.5e+10	1.13e+10

$\mathbf{e}_{15}$	$\mathbf{e}_{31}$	$\mathbf{e}_{33}$	ε_{11}^S	ε_{33}^S
2.56	-0.041	6.88	4.66e-09	3.78e-09

this is not avoidable, the effects of frequency dependencies are visible in the results. If one really wants to perform an exact three dimensional computer simulation one should not obviate a problem specific parameter adaptation, for which our developed scheme can easily be applied.

IX. CONCLUSION

The proposed method has turned out to be an indispensable tool for the generation of suitable material parameters for FE simulations. In addition, it proofs to be an appropriate procedure to determine material parameters with a high accuracy for newly developed piezoelectric ceramics. Its universality allows to consider all ponderable geometries and mode shapes of both lossless and lossy materials.

Further work on this subject is devoted to the simulation based identification of material parameters in piezoelectric compounds such as the determination of nonlinearities in the material parameters and those induced by the history of the materials, namely hysteresis.

REFERENCES

[1] O. Zienkiewicz and R. Taylor, *The Finite Element Method*. McGraw-Hill, 1994, vol. 1,2.
[2] K. Bathe, *Finite Element Procedures*. Prentice Hall, 1996.

[3] R. Lerch, “Simulation of piezoelectric devices by two- and three-dimensional finite elements,” *IIEEE Transactions on UFFC*, vol. 37, no. 3, pp. 233–247, 1990, iSSN 0885-3010.
[4] “IEEE Standard on Piezoelectricity,” 1985, iEEE/ANSI.
[5] “European standard prEN,” 50324-1:1998, 50324-2:1998, 50324-3:2001, 1998-2001.
[6] R. Holland and E. EerNisse, “Accurate measurement of coefficients in a ferroelectric ceramic,” *IEEE Transactions on Sonics and Ultrasonics*, vol. SU-16, no. 4, pp. 173–181, 1969.
[7] K. W. Kwok, H. L. W. Chan, and C. L. Choy, “Evaluation of the material parameters of piezoelectric materials by various methods,” *IEEEUFFC*, vol. 44, no. 4, pp. 733–742, 1997.
[8] S. Sherrit, H. D. Wiederick, and B. K. Mukherjee, “A complete characterization of the piezoelectric, dielectric, and elastic properties of Motorola PZT 3203 HD, including losses and dispersion,” *SPIE Proceedings*, 1997.
[9] J. G. Smits, “Iterative method for accurate determination of the real and imaginary parts of the materials coefficients of piezoelectric ceramics,” ser. IEEE Transactions on Sonics and Ultrasonics, vol. SU-23, no. 6, November 1976.
[10] X.-H. Du, Q.-M. Wang, and K. Uchino, “An accurate method for the determination of complex coefficients of single crystal piezoelectric resonators I: Theory,” vol. 51, pp. 227–235, 2004.
[11] M. Kaltenbacher, *Numerical Simulation of Mechatronic Sensors and Actuators*. Springer Berlin-Heidelberg-New York, 2004, iSBN: 3-540-20458-X.
[12] R. Holland, “Representation of dielectric, elastic, and piezoelectric losses by complex coefficients,” vol. 14, pp. 18–20, 1967.
[13] M. Hanke, “Regularizing properties of a truncated Newton–CG algorithm for nonlinear inverse problems,” *Numer. Funct. Anal. Optim.*, vol. 18, pp. 971–993, 1997.
[14] A. Rieder, “On the regularization of nonlinear ill-posed problems via inexact Newton iterations,” *Inverse Problems*, pp. 307–327, 1999.
[15] ——, “On convergence rates of inexact Newton regularizations,” *Numer. Math.*, vol. 88, 2001.
[16] H. W. Engl, M. Hanke, and A. Neubauer, *Regularization of Inverse Problems*. Dordrecht: Kluwer, 1996.
[17] M. Pernice and H. F. Walker, “NITSOL: A Newton iterative solver for nonlinear systems,” *SIAM J. Sci. Comput.*, vol. 19, pp. 302–318, 1998.
[18] B. Eicke, A. Louis, and R. Plato, “The instability of some gradient methods for ill-posed problems,” *Numer. Math*, 1990.
[19] B. Kaltenbacher, T. Lahmer, and V. Schulz, “Optimal experiment design for piezoelectric material tensor identification,” *Inverse Problems in Science and Engineering, submitted*, 2006.
[20] O. Schenk and K. Gärtner, “Solving unsymmetric sparse systems of linear equations with pardiso,” *Future Generation Computer Systems, available online www.sciencedirect.com*, p. 475487, 2004.
[21] Ferroperm, www.ferroperm-piezo.de, state: June, 2005.
[22] B. Kaltenbacher, T. Lahmer, and M. Mohr, “Pde based determination of piezoelectric material tensors,” *European Journal of Applied Mathematics*, 2006.

Barbara Kaltenbacher Prof. Dr., former head of junior research group ”Inverse Problems in Piezoelectricity” at department of sensor technology, University of Erlangen-Nuremberg, now full Professor at department of mathematics, university of Stuttgart, Germany ...
Manfred Kaltenbacher PD, Dr. techn. ... Researcher FEM,
Tom Lahmer Dipl. Math., researcher in ”Junior Research Group: Inverse Problems in Piezoelectricity”, supported by German Science Foundation DFG under grant Ka 1778/1, department of sensor technology, University of Erlangen-Nurenberg
Erich Leder Dipl. Ing. ...
Reinhard Lerch Prof. Dr.-Ing. Head of Department of Sensor Technology, Erlangen-Nurenberg, Germany ...